ACS Photonics

Article

pubs.acs.org/journal/apchd5

Nanowire-Aperture Probe: Local Enhanced Fluorescence Detection for the Investigation of Live Cells at the Nanoscale

Rune S. Frederiksen,[†] Esther Alarcon-Llado,[‡,⊥] Peter Krogstrup,[§] Laura Bojarskaite,[†] Nina Buch-Månson,[†] Jessica Bolinsson,[§] Jesper Nygård,[§] Anna Fontcuberta i Morral,[‡] and Karen L. Martinez*[,†]

[†]Bio-Nanotechnology and Nanomedicine Laboratory, Department of Chemistry & Nano-Science Center, University of Copenhagen, Universitetsparken 5, DK-2100 Copenhagen, Denmark

[‡]Laboratory of Semiconductor Materials, Institute of Materials, School of Engineering, École Polytechnique Fédérale de Lausanne, 1015 Lausanne, Switzerland

[§]Nano-Science Center & Center for Quantum Devices, Niels Bohr Institute, University of Copenhagen, Universitetsparken 5, DK-2100 Copenhagen, Denmark

[⊥]Center for Nanophotonics, FOM Institute AMOLF, Science Park 104, 1098XG Amsterdam, Netherlands

Supporting Information

ABSTRACT: Fluorescence microscopy has tackled many of the burning questions in cellular biology. Probing low-affinity cellular interactions remains one of the major challenges in the field to better understand cellular signaling. We introduce a novel approach—the nanowire-aperture probe (NAP)—to resolve biological signatures with a nanoscale resolution and a boost in light detection. The NAP takes advantage of the photonic properties of semiconductor nanowires and provides a highly localized excitation volume close to the nanowire surface. The probing region extends less than 20 nm into the solution, which can be exploited as a local light probe in fluorescence microscopy. This confined detection volume is especially advantageous in the study of cellular signaling at the cell membrane, as it wraps tightly around the nanowire. The nanowire acts as a local nanoaperture, both focusing the incoming excitation light and guiding photons emitted by the fluorophore. We demonstrate a 20-fold boost in signal-to-background sensitivity for single fluorophores and membrane-localized proteins in live cells. This work opens a completely new avenue for next-generation studies of live cells.

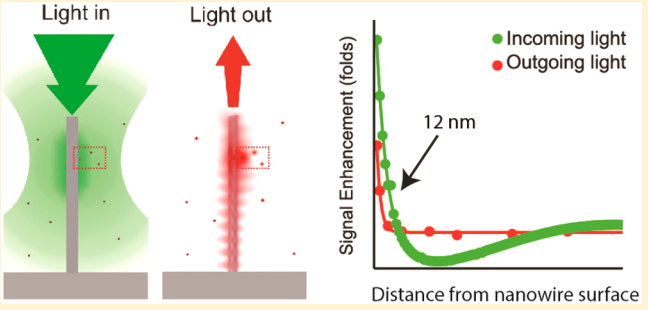

KEYWORDS: *nanoaperture, biosensing, localized excitation, nanoantenna, waveguiding, subdiffraction microscopy, cell, membrane protein, low-affinity interactions*

All physiological processes in the human body comprise interwoven chains of cellular signaling cascades, and a deeper knowledge of such signaling pathways is crucial for both biological and medical research.[1,2] Detailed spatiotemporal information about protein−protein interactions, which are the fundamental steps of any cellular cascade,[3,4] is typically obtained in live cells or in isolated systems (cell-free environment) via fluorescence-based imaging.[5−9]

Protein−protein interactions occur at length scales (∼10 nm) far below the diffraction limit barrier of optical microscopy (∼240 nm).[10] To overcome this resolution barrier, several techniques have been developed,[11] and at present two key strategies based on either fluorescence resonance energy transfer (FRET) or co-localization between two fluorescently labeled proteins are used. FRET is a very common method based on energy transfer between two fluorophores but requires an interaction between fluorophores that are closer than 10 nm.[12] In the case of co-localization of fluorescent molecules, several techniques have been developed to improve signal detection. Total internal reflection fluorescence (TIRF) microscopy reduces the excitation volume close to a surface (∼100 nm) and thus reduces the fluorescence background.[13] A spatial resolution down to 20 nm is possible using so-called super-resolution microscopes (e.g., stimulated emission depletion, stochastic optical reconstruction microscopy, and photoactivated localization microscopy),[14−16] which is an order of magnitude better than classical confocal microscopy. However, these approaches are expensive or labor intensive. The higher resolution comes at the cost of increased complexity of experimental conditions—such as reduced temporal resolution—and data analyses, and each approach requires the optimization of the fluorescence labeling of the proteins involved.

Nanostructures (e.g., nanoparticles, nanowires, nanochannels, and nanoholes) have established a new frontier for

Received: February 22, 2016
Published: June 10, 2016

DOI: 10.1021/acsphotonics.6b00126
ACS Photonics 2016, 3, 1208−1216

fluorescence-based studies by confining the detection volume in standard microscopy.[17−23] Exploring the modulation of the light pathway by nanostructures opens a window to new approaches overcoming the diffraction limitation of fluorescence-based studies,[24,25] which can be applied to address key low-affinity cellular interactions as it tackles low signal-to-background issues in standard probing techniques.[26,27] In particular, high aspect ratio dielectric nanowires have been shown to work as photonic structures that modulate light−matter interactions through several phenomena[28−31] including guiding,[32] emitting,[33,34] and collecting light.[35,36] Out of these phenomena, the principles behind the nanowire optical waveguiding effect suggest the potential of a highly localized nanowire-based aperture (nanowire-aperture), where a sub-diffraction probing volume around the nanowire is created and the radiation pattern of dipoles nearby is modified.

In addition to their optical features, arrays of nanostructures have been shown by us and others to have a great potential for the investigation of biological samples due to the high compatibility of their dimensions with cells (100−1000 times smaller) and with isolated proteins (area 10 000−20 000 times smaller than the surface of nanostructures). A broad range of proof-of-concepts has been illustrated in the past decade on purified proteins,[37,38] complex biological fluids,[37,38] and living cells for, for example, cell transfection, studies of single-cell signaling by fluorescence or electrophysiology, and diagnostics.[27,39−42]

While both features of nanostructures have a very strong potential for future applications, they have rarely been combined to explore biological systems, with one of the few examples being the work by Xie et al. with silica nanowires.[27,43,44] In this work we introduce a nanowire-aperture probe (NAP) based on GaAs nanowires. We show that when a NAP is in contact with cells, it can be exploited to study protein interactions in living cells at the nanoscale by tailoring the light through the unique photonic properties of these dielectric nanowires. We show that a NAP not only confines the probing volume to less than 20 nm from the nanowire surface when we use regular confocal microscopes but also enhances the signal-to-noise ratio of fluorescent processes within that volume. The working principles and potential of NAP are illustrated by both theoretical considerations and experiments. We give an example of application in live cells exploiting the NAP to reveal interactions between an intracellular protein and a membrane receptor.

RESULTS

Nanowire-Aperture Probe Setup. The essence of the NAP is the use of nanowires with a high refractive index vertically oriented on a substrate illuminated in a confocal microscope. The sample is placed in an aqueous solution, buoyant at a couple of micrometers from a coverslip. The advantage of the NAP is twofold: the probing volume is restricted to a biologically relevant distance (i.e., <20 nm) and a strong signal enhancement is obtained within that region. This is of considerable advantage for studying interactions at cell membranes, as they tend to tightly embrace nanowires.[45,46] The signal enhancement is a synergistic combination of a light up-concentrating power of the nanowire (i.e., the antenna effect) and the modulation of fluorophore emission by the presence of the nanowire. Figure 1 schematically describes these two phenomena, which will be explained in more detail in the next section.

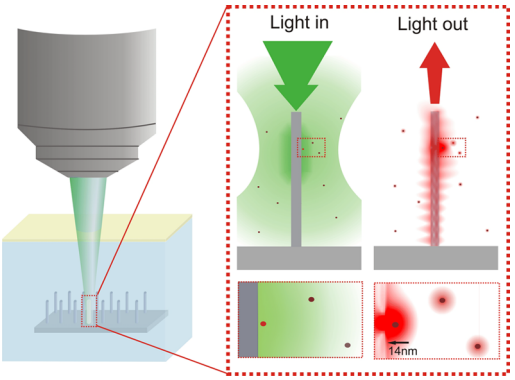

Figure 1. Mechanism of nanowire-aperture probe (NAP) impact on the light path. Schematic illustration of the nanowire array in a fluorescence confocal microscope. When focusing onto the NAP, the volume in close proximity to the nanowire surface (<40 nm) is much brighter than the rest of the laser excitation spot arising from the nanowire light self-concentrating power. In turn, fluorophores in close proximity to the nanowire surface (<14 nm) radiate predominantly into the high dielectric constant material (i.e., the nanowire). The nanowire then acts as a waveguide and directs most of the light toward the nanowire tip, where it outcouples and is emitted back toward the microscope objective lens.

Numerous nanowire materials can be used as NAPs. In this work, we focus on gallium arsenide (GaAs) nanowires grown on silicon substrates via the self-catalyzed vapor−liquid−solid mechanism,[47] with diameters of approximately 100 nm and lengths between 2 and 5 μm (see SI Figure S1). The motivation for using GaAs is due to its large refractive index ($n > 3$) and relatively small extinction coefficient at visible wavelengths, while offering excellent optical functionality. As will be explained in the following section, it is important for the NAP effect that the light efficiently couples to a guided mode. Depending on the refractive index of the material and embedding medium, nanowire diameter, and wavelength, the coupling is more or less effective and other modes can also exist.[48] GaAs nanowires of diameters smaller than 125 nm in water will support only a fundamental HE11 guided mode at the wavelengths of interest in this experiment. Further information on how size affects the photonic properties of the nanowires is found in the Supporting Information (section SI-3).

Tailoring the Electromagnetic Environment. A theoretical analysis is provided to outline the working principles of the NAP. We start by examining the interaction between the standing nanowire and the incoming excitation light, defined as a plane wave along the nanowire axis. Figure 2a shows the field energy distribution around the nanowire embedded in water under steady-state conditions. Most of the incoming light is concentrated close to the nanowire surface. This is due to the coupling of light into a guided mode of the nanowire (see section SI-3 for further information). In turn, the preferential light gathering at the nanowire creates a "dark region" next to the "bright" region in close proximity to the nanowire surface. As shown in the contour plots in Figure 2a, this "dark region" can extend up to 700 nm around the nanowire. In the zoom-in of Figure 2a, we show how light intensity in the bright region rapidly decays with distance to the nanowire surface (with a characteristic decay length of 45 nm from an exponential decay fit), due to the evanescent nature of the field at the nanowire−water interface. Figure 2b plots the quantitative increase in

DOI: 10.1021/acsphotonics.6b00126
ACS Photonics 2016, 3, 1208−1216

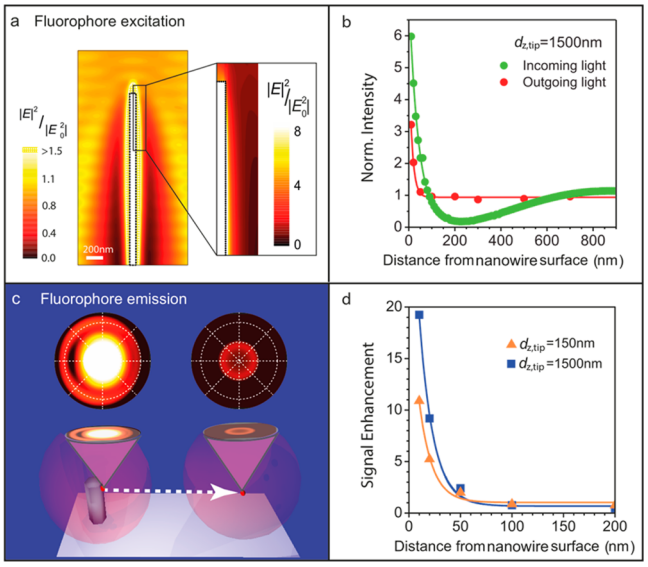

Figure 2. Simulations of the modulation of the light distribution in the proximity of the nanowire. (a) 2D map of the field energy density distribution around the GaAs nanowire under steady-state excitation conditions (see text for more details). A close-up of the nanowire tip is also shown to illustrate the strong confinement of a "bright" region at the nanowire surface. (b) Simulated signal enhancement given for incoming and outgoing light as a function of distance to the nanowire surface and distance $d_{z,tip}$ of 1500 nm to the nanowire tip. (c) Illustration of the aperture modulation of a dipole radiation by the presence of a GaAs nanowire. The two polar plots correspond to the radiation patterns of dipoles at 10 nm and far from the nanowire surface, respectively. Both plots are represented with the same color scale. (d) Representation of the strong confinement and total signal enhancement provided by a GaAs-based NAP close to the nanowire tip ($d_{z,tip}$ = 150 nm (orange)) and at 1500 nm from the tip (blue).

excitation light intensity as a function of distance to the nanowire surface at a distance ($d_{z,tip}$) of 1500 nm from the nanowire tip. We find an increase in photon flux at the nanowire surface of a factor of 6, which slightly varies along the axial position (see section SI-3).

We then look at the light emitted by dipoles located close to the nanowire surface (10 nm), which is a typical distance at which protein−protein interactions occur. Fluorophores emit photons isotropically unless the dipole is fixed. Thus, we have considered dipoles emitting in three orthogonal polarizations. Figure 2c compares the radiation pattern of such a dipole in solution and in the presence of a nanowire. In the latter, most of the emitted light is coupled into the nanowire, which at the same time effectively acts as a nanoscale optical fiber. The emitted photons are guided along the nanowire and outcoupled at the tip toward the objective lens with a significantly different angular pattern. As a result, the integrated power up to an angular aperture of 55 deg of light coming from such fluorophores is enhanced up to 3−4-fold, as indicated by the red dots in Figure 2b. The effect is strongly restricted to fluorophores in close proximity to the nanowire and with radially polarized emission (see section SI-2). We observe a strong correlation between light incoupling to a waveguide mode and signal detection, which corroborates that the enhancement is a combination of increased emission rate into the nanowire, waveguiding, and reduced angular radiation patterns of outcoupled light. As a result, a short characteristic decay length of 14 nm is obtained, by considering an exponential decay function.

Figure 2d convolutes the two photonic processes at two different axial positions, predicting a total fluorescence signal enhancement up to 20-fold for a single dipole emitter located at 10 nm from the nanowire surface. While total enhancement can reach a maximum of 25-fold at $d_{z,tip} \approx 1000$ nm, the average enhancement is around 20 for dipoles emitting at 500 nm from the tip and below (see SI Figure S3-1 for more detailed information on the axial dependence). Such enhancement decays exponentially with distance to the nanowire surface, with a decay length of ∼13 nm regardless of the axial position. This result elucidates the extremely confined probing volume of the NAP.

Experimental Demonstration of NAP Working Principle. On the basis of simulations, two different optical processes (confining incoming light and waveguiding of dipole emission) are responsible for the enhancement of signal detection in NAP-based fluorescence spectroscopy. We now provide experimental evidence of the combined phenomena by using a GaAs nanowire array on a silicon substrate. We have mapped the three-dimensional electromagnetic field distribution around a GaAs nanowire by immersing it in a solution of fluorescent dye (Alexa Fluor 647) and collecting the light emission in a confocal microscope, as illustrated in Figure 3a. No fluorescence signal was detected after washing the sample in

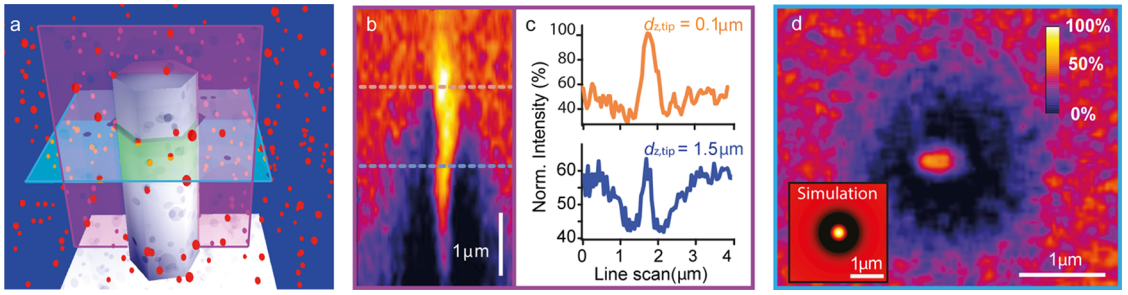

Figure 3. GaAs nanowires immersed in a fluorescent dye solution to map the three-dimensional electromagnetic field distribution, by measuring the fluorescence dye in solution (500 μM Alexa Fluor 647) surrounding the GaAs nanowire (excitation, 633 nm; emission, 670−690 nm) in a confocal microscope. (a) Scheme of a nanowire immersed into a dye solution with cross sections in the *xy*-plane (green) and *zx*-plane (pink), illustrating where the data in panels b and d are obtained. (b) Fluorescence side view (*xz*-plane) of the solution-immersed GaAs nanowire. (c) Line scans in the *xy*-plane through the nanowire, at $d_{z,tip}$ 150 nm (red) and 1500 nm (green) from the nanowire tip (intensities are normalized to max intensity in part b). (d) Fluorescence *z*-cut (*xy*-plane) at $d_{z,tip}$ = 1500 nm. Intensity is normalized to the max intensity. Inset: Simulated intensity map data obtained with similar condition and location on the nanowire.

DOI: 10.1021/acsphotonics.6b00126
ACS Photonics 2016, 3, 1208−1216

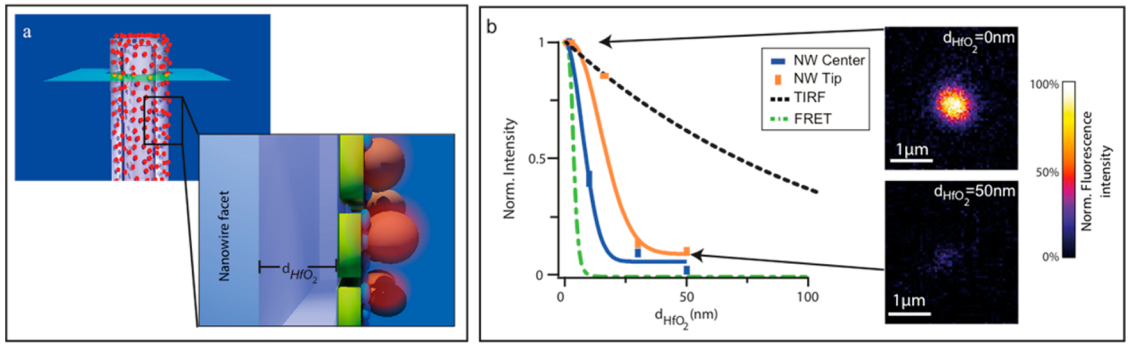

Figure 4. Tuning the nanowire−fluorophore distance by adding a HfO_2 layer between the nanowire and the fluorophore. (a) Illustration of streptavidin-Alexa Fluor 647 binding with the receptor (BSA-biotin) immobilized on the nanowire. (b) Fluorescence signal—normalized to intensity without HfO_2—as a function of HfO_2 thickness to illustrate the detection volume from the nanowire compared to a TIRF microscope (penetration depth of 90 nm) and FRET (Föster distance of 5 nm). Thick lines correspond to exponential decay fits to experimental data. Curves associated with TIRF and FRET techniques are theoretical exponential profiles. Insets show raw fluorescence *xy*-plane images of a single nanowire with respectively 0 and 50 nm of HfO_2 between the nanowire and fluorophore.

a buffer solution, indicating that the fluorophores were not bound to the nanowires (see SI Figure S4).

The *xy*-image (Figure 3b) shows a high fluorescence intensity along the nanowire and a region with reduced fluorescence signal (referred to as "shadow" in the rest of the article) in the surrounding of the nanowire that increases in width along the light path as predicted by theory (Figure 2a). This is further illustrated in Figure 3c and d. The line scans in Figure 3c show that both the enhancement and the "shadow" depend on the axial position along the nanowire, as predicted by simulations. The *z*-cut (*xy*-plane) of the emission pattern at $d_{z,tip}$ = 1.5 μm from Figure 3d also shows a clear enhancement of light detection at the nanowire position surrounded by the dark shadow around it, which highlights the relevance of this technique to probe fluorophore emission close to a nanowire with low background noise. This shadow originates from the strong coupling of light into the nanowire and can have a diameter of up to 1300 nm at the bottom, which is much larger than a diffraction-limited spot in regular microscopes. We have simulated a *z*-cut of detected signal focusing at the same $d_{z,tip}$ by taking into account excitation and emission of light as described in the previous section. The resulting intensity map convoluted with a Gaussian PSF of the confocal microscope is shown in the inset of Figure 3d, and it is in excellent agreement with the measurements. These results further illustrate the role of the nanowire as an extremely small optical aperture as predicted by theory.

Determination of the Subdiffraction Light Confinement. To measure the detection volume around the nanowire, we have tuned the distance between the nanowire and fluorophore using a controlled layer of optically transparent hafnium oxide (HfO_2), as illustrated in Figure 4a. In this particular experiment, fluorescent proteins (streptavidin-Alexa Fluor 647) were adsorbed to the nanowire surface (using BSA-biotin). The integrated signal as a function of HfO_2 thickness is displayed in Figure 4b for two axial positions along the nanowire (close to the tip and at around 1500 nm below). As expected from the simulations, the fluorescence signal decreases rapidly within the first 50 nm and is independent of the axial position. This effect is not due to the optical properties of HfO_2 nor quenching induced by HfO_2 (see SI Figures S5 and S6). The experimental decay length fitted to a Gaussian decay depends on the axial position and is 8 and 12 nm for positions at midheight and tip of the nanowire, respectively, which is again in good agreement with the theoretical prediction of 13 nm. This corresponds to a NAP probing volume of 0.01 μm^3.

Such a probing distance is much smaller than the TIRF, which is widely used for the investigation of biological samples and has a typical decay length of 90 nm, as illustrated in Figure 4b. The NAP volume is highly confined in 2D (in the *xy*-plane), making it optimal to study biological interactions at the nanowire surface. The NAP probing distance thus appears as a technique filling the gap between TIRF and FRET techniques, which is ideal for studying biological interactions at both sides of a cell membrane, the latter being around 4−5 nm in thickness. In addition, a NAP is an easy to use setup compatible with a standard confocal microscope.

Evaluation of the Probing Effects for Biosensing. Probing low-affinity interactions is still a major challenge in fluorescence microscopy. Because of the equilibrium between bound and free fluorescent molecules, a large excess of fluorescent molecules are in solution during the measurements and thereby contribute to the fluorescence background. Here we evaluate the potential of the NAP by comparing the signal-to-background (SBR) of the NAP with that of TIRF microscopy, a common technique to reduce the background fluorescence signal in biological studies.

This study is conducted under relevant biosensing conditions, i.e., at a high background signal, where it is challenging to measure binding events (micromolar concentrations of fluorescent molecules). We monitored the binding of fluorescently labeled streptavidin present in high excess in solution (4 μM) to a surface prefunctionalized with BSA-biotin.

The specific signal obtained is 704% and 55% with the NAP and TIRF, respectively. Thus, using the NAP instead of TIRF leads to a 12.8-fold enhancement of the specific signal detected (see Figure S7). These results highlight the potential of a NAP for tackling low-intensity specific signals in the presence of high background fluorescence, which is typically the case in cell studies, where intracellular labeling of proteins and resulting fluorescence signals are hard to control.

One should note that the 704% SBR cannot be directly compared to the 20-fold enhancement predicted by our theoretical calculations. Our simulation gives a 20 times increase in signal from a single fluorophore next to a GaAs nanowire with respect to a fluorophore suspended in solution. Even if the whole probing volume was considered instead of a single emitter, the background signal is difficult to account for

DOI: 10.1021/acsphotonics.6b00126
ACS Photonics 2016, 3, 1208−1216

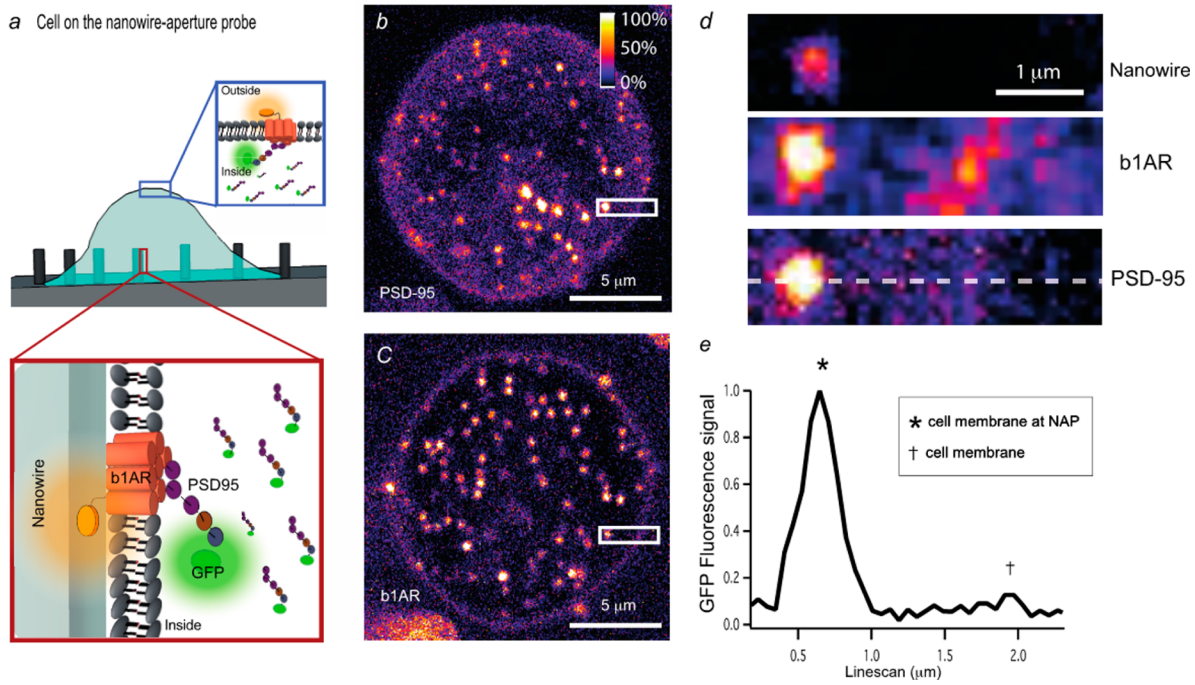

Figure 5. Detection of low signal-to-background PSD95:b1AR interaction by exploitation of subdiffraction nanowire aperture probing. (a) Illustration of the investigated interaction: Cytosolic scaffold protein PSD-95 (fused to GFP) binds the C-terminal tail of b1AR (labeled with BG-547 through an extracellular SNAP-tag) and is recruited to the membrane. Low receptor concentration results in low PSD-95 recruitment to the membrane, thus creating a low signal (PSD-95 at the membrane) to noise (PSD-95 in the cytosol) ratio. (b, c) Confocal slices through a cell interfaced with a NAP as seen in the PSD-95-GFP (b) and b1AR (c) channels. (d) Zoom-ins of a region (indicated in b, c) with a single nanowire close to the border of the cell showing a clear co-localization of the PSD-95, b1AR, and nanowire (photoluminescence) signals. (e) Line scan of the PSD-95 signal across the zoom-in of d. The positions of the nanowire (*) and the regular cell membrane (†) are indicated.

in the analysis. In order to decouple the two effects, we did measurements on a second nanostructured system that does not produce a significant signal enhancement (i.e., using a material with a refractive index close to that of water). To this end, biotin-functionalized SiO_2 nanobeads were taken as reference material to bind the fluorescent streptavidin. The specific signal of functionalized SiO_2 beads in the same highly concentrated solution was only 5%, in agreement with simulations where almost no enhancement (maximum local enhancement of 1.5) by the bead is predicted. Comparing the experimental signal increase with the background signal on the two nanostructures (704% and 5%), a 140-fold enhancement is achieved using the NAP. This is in very good agreement with that found by simulations (160-fold), where photonic effects and surface area of the two nanostructures were considered (see SI Table S1 and Figure S8 for more information).

This example highlights the key importance of choosing the right material as a NAP; for example, SiO_2 will not produce a significant effect due to its refractive index being too close to that of water. In such case, the nanostructure does not behave like a waveguide. On the other hand, the value of the extinction coefficient is also important. The smaller the absorption, the higher the portion of light traveling inside the nanowire that will reach the tip and outcouple to free space. To stress this point, we have also measured the SBR of biotin-functionalized InAs nanowires in the same experimental conditions. InAs has a similar refractive index coefficient to GaAs, but much stronger light absorption properties. We obtained for InAs-based NAP 17 times less signal than in the case of GaAs (see SI S9).

NAP-Mediated Resolution of a Low-Affinity Protein–Protein Interaction in Live Cells. Finally, to validate the potential of the NAP for live cell investigations, we probed a low-affinity interaction between a membrane protein and an intracellular protein at the plasma membrane. This is one of the most challenging imaging cases due to a high background signal as a result of the low affinity. Scaffold proteins are essential intracellular proteins involved in the coordination of signal transduction cascades. Their affinities for membrane proteins have so far only been measured on isolated proteins and isolated cell membranes using biochemical and biophysical methods, which revealed low-affinity interactions (i.e., in the μM range).[49] Here, the NAP could be a powerful tool to increase the knowledge about scaffolding proteins, their interaction with other intracellular proteins and membrane proteins, and their role in cell signaling, which are still poorly elucidated today.

As a model interaction for this study, we imaged the interactions in cells of a G-protein-coupled receptor, beta-1 adrenergic receptor (b1AR), with the intracellular scaffold protein postsynaptic density protein 95 (PSD-95).[50] PSD-95 is the most abundant scaffold protein in the postsynaptic density of excitatory glutamatergic synapses and is known to be important for the regulation of synaptic plasticity, learning, and memory.[51−53]

We have previously shown that b1AR interacts specifically via its C-terminal tail with a PDZ domain of PSD-95.[49] This specific interaction results in the partial recruitment of PSD-95 to the cell membrane, which is difficult to detect with classical microscopy techniques due to a high background signal from the nonbound cytosolic PSD-95 (see confocal imaging of cells on coverslips in SI Figure S10). Such challenging conditions are

DOI: 10.1021/acsphotonics.6b00126
ACS Photonics 2016, 3, 1208−1216

perfect for the evaluation of the potential of the NAP for cell imaging.

We first verified that cells can be interfaced with GaAs nanowires, coated with a nanometer thin layer of HfO_2 (see SEM image in Figure S11). The cell viability was as good as on glass surfaces (see viability data in SI section S12), and the cell interface was similar to what has been observed on various arrays of high aspect ratio nanostructures.[39] The wrapping of the cell membrane along part of the nanowire, due to the density of nanowires and predicted by our previous studies,[46,54] results in a close interface between the cell plasma membrane and the nanowire (SI S13).

For this study, the intracellular PSD-95 was fused to GFP and b1AR was labeled via an extracellular SNAP-tag with BG-547 (Figure 5a) as in previous studies.[45,49] The distance between the two fluorophores located on each side of the plasma membrane is larger than the Förster distance between them, preventing FRET effects. Thus, the interaction may be observed only through co-localization of the two signals.

The position of nanowires was detected through their photoluminescence, excited at 633 nm, and thus did not interfere with the detection of the PSD-95 and b1AR signals. The interaction between PSD-95 and b1AR was measured as the signal of receptor-bound PSD-95 at the cell membrane compared to the background signal of nonbound cytosolic PSD-95 (Figure 5b–d, SI S13). The NAP-mediated enhancement of the detection of PSD-95:b1AR interaction is clearly visible from the bright fluorescent signal of PSD-95 at the interface with nanowires.

In a single experiment, it was possible to compare quantitatively the SBR obtained by the NAP and classical confocal microscopy by measuring at distinct locations in a single cell (limiting thereby heterogeneity of signals due to heterogeneous cell populations). Line scans across positions at the cell membrane in close contact with or away from nanowires were used to evaluate the fluorescence intensities corresponding to receptor-bound PSD-95 and the cytosolic signal in between (i.e., intracellular background signal) (Figure 5d,e). The SBR of PSD-95 is 20 fold higher when the membrane is in contact with a nanowire benefiting from NAP (i.e., an SBR of 10.1 and 0.5, respectively, at the nanowire and at the cell membrane in the absence of a nanowire). Control experiments on another type of nanowires confirmed that this enhancement was due to the optical properties of GaAs nanowires and not an artifact of, for example, a different geometry of the membrane at the nanowire (SI S14). More examples of line scans across the nanowires in Figure 5b are given in Figure S15.

Using a NAP, we bring the PSD-95 recruitment signal clearly out of the background signal, thus resolving otherwise unclear PSD-95:b1AR interactions. Hence, the NAP presents an enormous potential for future applications in bioimaging.

CONCLUSION

We have shown that a NAP provides a highly localized detection volume at the nanowire surface, which can be exploited as a local light source in biosensing. We demonstrate how a NAP creates a 3D illumination profile extending less than 20 nm into the solution. A reduced detection volume is obtained by the photonic interaction with a high refractive index nanowire. The nanowire acts as an aperture, both focusing the incoming excitation photon flux and guiding the fluorophore photon emission. We exploit the NAP to study low-affinity interactions at the membrane of living cells with a boosted signal-to-background ratio of 20-fold.

The NAP is compatible with wide-field and confocal microscopes, without any modification of the instrumental setup. It is based on the simple addition of a small-sized chip to the sample chamber. This provides a single image both at standard imaging resolution and at super-resolution at specific locations within the sample due to the small aperture given by the nanowire.

The NAP thus opens up novel perspectives for the real-time evaluation of molecular interactions in cells. It will be particularly suitable for the study of interactions taking place in cell membranes (plasma and organelles)[45,55] or to investigate any molecular interactions with one of the partners immobilized on the nanowire.[38,40] As an example, we believe that NAPs have a great potential for selective photoactivation of proteins in live cells, which enables following the protein dynamics in living cells.[56,57]

MATERIALS AND METHODS

Nanowire Growth. The GaAs nanowires were grown by molecular beam epitaxy on oxidized Si(111) with 100 nm apertures using a self-catalyzed method, as previously described by Krogstrup et al.[47] . The Au seeded GaAs nanowire chips was produced as described by Kolasinski.[58]

The HfO_2 layers were deposited via atomic layer deposition at 150 °C using tetrakis(methylamino)hafnium and water vapor, 0.2 and 0.02 s pulses, respectively, and 45/45 s purge times, respectively.

Nanowire Functionalization with BSA-Biotin and Streptavidin. Nanowire arrays were functionalized with 0.1 mg/mL BSA-biotin (Sigma-Aldrich) and 1 mL of Alexa Fluor 647 streptavidin conjugate in 0.01 M PBS buffer (Life Technologies) as described in Rostgaard et al.[38]

Flp-In T-Rex 293 Cell Culture. Cultures of stable Flp-In T-Rex 293 cells (Life Technologies) expressing PSD-95-GFP constitutively and SNAP-b1AR under induction were maintained at 37 °C, 5% CO_2, and >95% humidity and cultured in DMEM/F-12 + Glutamax-I medium (Gibco) supplemented with 10% fetal bovine serum (Gibco), 100 μg/mL hygromycin, 15 μg/mL blasticidin, and 200 μg/mL Geneticin (=$DMEM_{T\text{-}Rex}$).

SNAP-b1AR Labeling. Just before interfacing the cells with nanowires and imaging, the SNAP-b1AR receptor in cells was labeled for 10 min at 37 °C with 5 μM BG-547 (New England Biolabs) dye, as previously described,[45,49] in $DMEM_{T\text{-}Rex}$ and then washed three times in serum-free DMEM/F-12 HEPES medium (Gibco).

Interfacing Cells with Nanowire Arrays. 1 mL cell suspension in serum-free DMEM/F-12 HEPES medium was transferred to a sterilized nanowire array placed in a 24-well plate. The plate was swirled gently to distribute the cells and incubated for 30 min at 37 °C, 5% CO_2, and >95% humidity before imaging. The expression of SNAP-b1AR was induced with 0.01 μg/mL tetracycline 24 h before interfacing.

Fluorescence Imaging. Confocal laser scanning microscopy imaging was performed on an inverted confocal laser scanning microscope (Leica TCS SP5). For the live-cell imaging (Figure 5), a 63× magnification, water-immersion objective with a 1.2 numerical aperture was used, and imaging was performed in serum-free DMEM/F-12 HEPES medium. For the cell-free measurements (Figures 3 and 4), a 100×

DOI: 10.1021/acsphotonics.6b00126
ACS Photonics 2016, 3, 1208–1216

magnification, oil-immersion objective with a 1.4 numerical aperture was used.

The fluorophores were excited and the emission was collected by a photomultiplier tube at the following excitation: emission wavelengths ex488: em508−540 nm (PSD-95, GFP), ex543 nm: em560−600 nm (SNAP-b1AR, BG-547), and ex633 nm: em650−700 nm (streptavidin, Alexa Fluor 647). The nanowire photoluminescence was detected at ex633 nm: em730−800 nm.

Complying with the Nyquist rate for optimal imaging conditions, Z-stacks were collected with a pinhole of one airy unit, and a pixel and step size of approximately 50 × 50 nm^2 and 130 nm, respectively.

Quantification of Fluorescence Signals. Quantification of fluorescence signals was performed with ImageJ software. The nanowire signals were measured with a ROI of 10 pixels around each nanowire, where each plane was fitted to a 2D Gaussian. The fluorescence signal was measured as the Gaussian volume using the fwhm and the amplitude of the Gaussian. The line scan used in Figure 5 was an average over 5 pixels.

Quantification of Specific Signals. The specific signal is defined as $I_{signal} = I_{total}/I_{nonspecific} - 1$, where $I_{nonspecific}$ is the nonspecific signal. This signal was evaluated experimentally using fluorescent streptavidin saturated with biotin and thereby not able to bind to the surface coated with BSA.biot.

Total Internal Reflection Fluorescence Microscopy. TIRF imaging was performed on a spinning disk confocal microscope (CSU-X1) TIRF. The coverslips were functionalized with 0.1 mg/mL BSA-biotin (Sigma-Aldrich) and 4 μM Alexa Fluor 647 streptavidin conjugate in 0.01 M PBS buffer (Life Technologies) as described in Rostgaard et al.[38] As control the nonspecific signal was measured, where the signal from straptavidin preblocked with biotin is taken as the nonspecific signal. The fluorescence from streptavidin Alexa Fluor 647 was measured using the BP629/62 FILTER CUBE.

Theoretical Simulations. Simulations were carried out by evolving Maxwell's equations over finite time steps on a single GaAs nanowire vertically standing on a SiO_2/Si substrate, as in the experiments. In the following, we describe how the NAP tailors the nanowire's electromagnetic environment through simulating both the incoming excitation light flux and the outgoing fluorophore photon emission separately.

GaAs nanowires on a silicon substrate were set to 100 nm in diameter and 3 μm in length and immersed in water. The finite-difference time-domain software package MEEP was used to model the electromagnetic response. For simulating the excitation field energy density distribution, a plane monochromatic (λ = 633 nm) wave was used as a light source propagating along the vertical direction. Perfectly matching layers around the cell were included to avoid scattering at the boundaries. Monochromatic single dipole emitters (λ = 680 nm) were used to simulate the fluorophore emission. The power flux equivalent for an objective lens with an angular aperture of 60° was measured at a distance of 325 nm from the nanowire tip. The refractive index and extinction coefficient of GaAs and silicon were set to n_{GaAs} = 3.8571/3.794 94, k_{GaAs} = 0.198 14/0.157 79, n_{Si} = 3.882/3.808 36, and k_{Si} = 0.0196/0.013 27 for λ = 633/680 nm, respectively. n = 1.331 was used for water.

■ ASSOCIATED CONTENT

Supporting Information

The Supporting Information is available free of charge on the ACS Publications website at DOI: 10.1021/acsphotonics.6b00126.

Additional figures (PDF)

■ AUTHOR INFORMATION

Corresponding Author

*E-mail: martinez@nano.ku.dk (K. L. Martinez).

Notes

The authors declare no competing financial interest.

■ ACKNOWLEDGMENTS

We thank Shivendra Upadhyay for technical support. For financial support, we thank the Danish Agency for Science Technology and Innovation (Innovation Fund Denmark - ANaCell project), UNIK Synthetic Biology (funded by the Danish Ministry for Science, Technology and Innovation), the Danish Advanced Technology Foundation, the ERC Stg 'UpCon', the Swiss National Fund "Ambizione Energy", NCCR QSIT, and the Lundbeck Center for Biomembrane and Nanomedicine.

■ REFERENCES

(1) Sun, Y.; Hays, N. M.; Periasamy, A.; Davidson, M. W.; Day, R. N. *Monitoring Protein Interactions in Living Cells with Fluorescence Lifetime Imaging Microscopy*, 1st ed.; Elsevier Inc., 2012; Vol. *504*.

(2) Todd; Gomez. Enzyme Kinetics Determined Using Calorimetry: A General Assay for Enzyme Activity? *Anal. Biochem.* **2001**, *296*, 179−187.

(3) Ho, Y.; Gruhler, A.; Heilbut, A.; Bader, G. D.; Moore, L.; Adams, S.-L.; Millar, A.; Taylor, P.; Bennett, K.; Boutilier, K.; Yang, L.; Wolting, C.; Donaldson, I.; Schandorff, S.; Shewnarane, J.; Vo, M.; Taggart, J.; Goudreault, M.; Muskat, B.; Alfarano, C.; Dewar, D.; Lin, Z.; Michalickova, K.; Willems, A. R.; Sassi, H.; Nielsen, P. A.; Rasmussen, K. J.; Andersen, J. R.; Johansen, L. E.; Hansen, L. H.; Jespersen, H.; Podtelejnikov, A.; Nielsen, E.; Crawford, J.; Poulsen, V.; Sørensen, B. D.; Matthiesen, J.; Hendrickson, R. C.; Gleeson, F.; Pawson, T.; Moran, M. F.; Durocher, D.; Mann, M.; Hogue, C. W. V; Figeys, D.; Tyers, M. Systematic Identification of Protein Complexes in Saccharomyces Cerevisiae by Mass Spectrometry. *Nature* **2002**, *415*, 180−183.

(4) Gavin, A.-C.; Bösche, M.; Krause, R.; Grandi, P.; Marzioch, M.; Bauer, A.; Schultz, J.; Rick, J. M.; Michon, A.-M.; Cruciat, C.-M.; Remor, M.; Höfert, C.; Schelder, M.; Brajenovic, M.; Ruffner, H.; Merino, A.; Klein, K.; Hudak, M.; Dickson, D.; Rudi, T.; Gnau, V.; Bauch, A.; Bastuck, S.; Huhse, B.; Leutwein, C.; Heurtier, M.-A.; Copley, R. R.; Edelmann, A.; Querfurth, E.; Rybin, V.; Drewes, G.; Raida, M.; Bouwmeester, T.; Bork, P.; Seraphin, B.; Kuster, B.; Neubauer, G.; Superti-Furga, G. Functional Organization of the Yeast Proteome by Systematic Analysis of Protein Complexes. *Nature* **2002**, *415*, 141−147.

(5) Leake, M. C.; Chandler, J. H.; Wadhams, G. H.; Bai, F.; Berry, R. M.; Armitage, J. P. Stoichiometry and Turnover in Single, Functioning Membrane Protein Complexes. *Nature* **2006**, *443*, 355−358.

(6) Levskaya, A.; Weiner, O. D.; Lim, W. a; Voigt, C. a. Spatiotemporal Control of Cell Signalling Using a Light-Switchable Protein Interaction. *Nature* **2009**, *461*, 997−1001.

(7) Sohn, H. W.; Tolar, P.; Brzostowski, J.; Pierce, S. K. A Method for Analyzing Protein-Protein Interactions in the Plasma Membrane of Live B Cells by Fluorescence Resonance Energy Transfer Imaging as Acquired by Total Internal Reflection Fluorescence Microscopy. *Methods Mol. Biol.* **2010**, *591*, 159−183.

DOI: 10.1021/acsphotonics.6b00126
ACS Photonics 2016, 3, 1208−1216

(8) Miyashita, T. Confocal Microscopy for Intracellular Co-Localization of Proteins. *Methods Mol. Biol.* **2004**, *261*, 399−410.
(9) Best, M. Click Chemistry and Bioorthogonal Reactions: Unprecedented Selectivity in the Labeling of Biological Molecules. *Biochemistry* **2009**, *48*, 6571−6584.
(10) Nasse, M. J.; Woehl, J. C. Realistic Modeling of the Illumination Point Spread Function in Confocal Scanning Optical Microscopy. *J. Opt. Soc. Am. A* **2010**, *27*, 295−302.
(11) Cordes, S. W. H.; Hell, J. S.; Bates, B.; Zhuang, Z.; Heintzmann, H.; Booth, J. B.; Bewersdorf, B.; Shtengel, S.; Hess, H.; Tinnefeld, T.; Honigmann, H.; Jakobs, J.; Testa, T.; Cognet, C. The 2015 Super-Resolution Microscopy Roadmap. *J. Phys. D: Appl. Phys.* **2015**, *48*, 443001.
(12) Zheng, J. Spectroscopy-Based Quantitative Fluorescence Resonance Energy Transfer Analysis. *Methods Mol. Biol.* **2006**, *337*, 65−77.
(13) AMBROSE, E. J. A Surface Contact Microscope for the Study of Cell Movements. *Nature* **1956**, *178*, 1194−1194.
(14) Rust, M. J.; Bates, M.; Zhuang, X. Sub-Diffraction-Limit Imaging by Stochastic Optical Reconstruction Microscopy (STORM). *Nat. Methods* **2006**, *3*, 793−796.
(15) Eggeling, C.; Ringemann, C.; Medda, R.; Schwarzmann, G.; Sandhoff, K.; Polyakova, S.; Belov, V. N.; Hein, B.; von Middendorff, C.; Schönle, A.; Hell, S. W. Bro. *Nature* **2009**, *457*, 1159−1162.
(16) Brown, D. A.; London, E. Structure and Function of Sphingolipid- and Cholesterol-Rich Membrane Rafts. *J. Biol. Chem.* **2000**, *275*, 17221−17224.
(17) Mannion, J. T.; Craighead, H. G. Nanofluidic Structures for Single Biomolecule Fluorescent Detection. *Biopolymers* **2007**, *85*, 131−143.
(18) Levene, M. J.; Korlach, J.; Turner, S. W.; Foquet, M.; Craighead, H. G.; Webb, W. W. Zero-Mode Waveguides for Single-Molecule Analysis at High Concentrations. *Science* **2003**, *299*, 682−686.
(19) Punj, D.; Mivelle, M.; Moparthi, S. B.; van Zanten, T. S.; Rigneault, H.; van Hulst, N. F.; Garcia-Parajo, M. F.; Wenger, J. A Plasmonic ⁄antenna-in-Box⁄' Platform for Enhanced Single-Molecule Analysis at Micromolar Concentrations. *Nat. Nanotechnol.* **2013**, *8*, 512−516.
(20) Kramer, A.; Trabesinger, W.; Hecht, B.; Wild, U. P. Optical near-Field Enhancement at a Metal Tip Probed by a Single Fluorophore. *Appl. Phys. Lett.* **2002**, *80*.165210.1063/1.1453479
(21) Bharadwaj, P.; Anger, P.; Novotny, L. Nanoplasmonic Enhancement of Single-Molecule Fluorescence. *Nanotechnology* **2007**, *18*, 44017.
(22) Lohmüller, T.; Iversen, L.; Schmidt, M.; Rhodes, C.; Tu, H.-L.; Lin, W.-C.; Groves, J. T. Single Molecule Tracking on Supported Membranes with Arrays of Optical Nanoantennas. *Nano Lett.* **2012**, *12*, 1717−1721.
(23) Puchkova, A.; Vietz, C.; Pibiri, E.; Wünsch, B.; Sanz Paz, M.; Acuna, G. P.; Tinnefeld, P. DNA Origami Nanoantennas with over 5000-Fold Fluorescence Enhancement and Single-Molecule Detection at 25 μM. *Nano Lett.* **2015**, *15*, 8354−8359.
(24) Gérard, D.; Wenger, J.; Bonod, N.; Popov, E.; Rigneault, H.; Mahdavi, F.; Blair, S.; Dintinger, J.; Ebbesen, T. Nanoaperture-Enhanced Fluorescence: Towards Higher Detection Rates with Plasmonic Metals. *Phys. Rev. B: Condens. Matter Mater. Phys.* **2008**, *77*, 045413.
(25) Blom, H.; Kastrup, L.; Eggeling, C. Fluorescence Fluctuation Spectroscopy in Reduced Detection Volumes. *Curr. Pharm. Biotechnol.* **2006**, *7*, 51−66.
(26) Wenger, J.; Rigneault, H. Photonic Methods to Enhance Fluorescence Correlation Spectroscopy and Single Molecule Fluorescence Detection. *Int. J. Mol. Sci.* **2010**, *11*, 206−221.
(27) Xie, C.; Hanson, L.; Cui, Y.; Cui, B. Vertical Nanopillars for Highly Localized Fluorescence Imaging. *Proc. Natl. Acad. Sci. U. S. A.* **2011**, *108*, 3894−3899.
(28) Wu, P. M.; Anttu, N.; Xu, H. Q.; Samuelson, L.; Pistol, M.-E. Colorful InAs Nanowire Arrays: From Strong to Weak Absorption with Geometrical Tuning. *Nano Lett.* **2012**, *12*, 1990−1995.
(29) Grange, R.; Brönstrup, G.; Kiometzis, M.; Sergeyev, A.; Richter, J.; Leiterer, C.; Fritzsche, W.; Gutsche, C.; Lysov, A.; Prost, W.; Tegude, F.-J.; Pertsch, T.; Tünnermann, A.; Christiansen, S. Far-Field Imaging for Direct Visualization of Light Interferences in GaAs Nanowires. *Nano Lett.* **2012**, *12*, 5412−5417.
(30) Zhu, J.; Yu, Z.; Burkhard, G. F.; Hsu, C.-M.; Connor, S. T.; Xu, Y.; Wang, Q.; McGehee, M.; Fan, S.; Cui, Y. Optical Absorption Enhancement in Amorphous Silicon Nanowire and Nanocone Arrays. *Nano Lett.* **2009**, *9*, 279−282.
(31) Zhu, J.; Hsu, C.-M.; Yu, Z.; Fan, S.; Cui, Y. Nanodome Solar Cells with Efficient Light Management and Self-Cleaning. *Nano Lett.* **2010**, *10*, 1979−1984.
(32) Law, M.; Sirbuly, D. J.; Johnson, J. C.; Goldberger, J.; Saykally, R. J.; Yang, P. Nanoribbon Waveguides for Subwavelength Photonics Integration. *Science* **2004**, *305*, 1269−1273.
(33) Grzela, G.; Panuagua Dominguez, R.; Barten, T.; Fontana, Y.; Sanchez Gil, J. a; Gomez Rivas, J.; Paniagua-Domínguez, R.; Barten, T.; Fontana, Y.; Sánchez-Gil, J. A.; Gómez Rivas, J. Nanowire Antenna Emission. *Nano Lett.* **2012**, *12*, 5481−5486.
(34) Yan, R.; Gargas, D.; Yang, P. Nanowire Photonics. *Nat. Photonics* **2009**, *3*, 569−576.
(35) Colombo, C.; Krogstrup, P.; Nygård, J.; Brongersma, M. L.; Morral, A. F. I. Engineering Light Absorption in Single-Nanowire Solar Cells with Metal Nanoparticles. *New J. Phys.* **2011**, *13*, 123026.
(36) Frederiksen, R. S.; Alarcon-Llado, E.; Madsen, M. H.; Rostgaard, K. R.; Krogstrup, P.; Vosch, T.; Nygård, J.; Fontcuberta i Morral, A.; Martinez, K. L.; Nyga, J.; Fontcuberta, A.; Martinez, K. L. Modulation of Fluorescence Signals from Biomolecules along Nanowires Due to Interaction of Light with Oriented Nanostructures. *Nano Lett.* **2015**, *15*, 176−181.
(37) Krivitsky, V.; Hsiung, L.-C.; Lichtenstein, A.; Brudnik, B.; Kantaev, R.; Elnathan, R.; Pevzner, A.; Khatchtourints, A.; Patolsky, F. Si Nanowires Forest-Based On-Chip Biomolecular Filtering, Separation and Preconcentration Devices: Nanowires Do It All. *Nano Lett.* **2012**, *12*, 4748−4756.
(38) Rostgaard, K. R.; Frederiksen, R. S.; Liu, Y.-C. C.; Berthing, T.; Madsen, M. H.; Holm, J.; Nygård, J.; Martinez, K. L. Vertical Nanowire Arrays as a Versatile Platform for Protein Detection and Analysis. *Nanoscale* **2013**, *5*, 10226−10235.
(39) Bonde, S.; Buch-Månson, N.; Rostgaard, K. R.; Andersen, T. K.; Berthing, T.; Martinez, K. L. Exploring Arrays of Vertical One-Dimensional Nanostructures for Cellular Investigations. *Nanotechnology* **2014**, *25*, 362001.
(40) Chiappini, C.; Martinez, J. O.; De Rosa, E.; Almeida, C. S.; Tasciotti, E.; Stevens, M. M. Biodegradable Nanoneedles for Localized Delivery of Nanoparticles in Vivo: Exploring the Biointerface. *ACS Nano* **2015**, *9*, 5500−5509.
(41) Peng, J.; Garcia, M. A.; Choi, J.; Zhao, L.; Chen, K.; Bernstein, J. R.; Peyda, P.; Hsiao, Y.-S.; Liu, K. W.; Lin, W.-Y.; Pyle, A. D.; Wang, H.; Hou, S.; Tseng, H.-R. Molecular Recognition Enables Nano-substrate-Mediated Delivery of Gene-Encapsulated Nanoparticles with High Efficiency. *ACS Nano* **2014**, *8*, 4621−4629.
(42) Robinson, J. T.; Jorgolli, M.; Shalek, A. K.; Yoon, M.-H.; Gertner, R. S.; Park, H. Vertical Nanowire Electrode Arrays as a Scalable Platform for Intracellular Interfacing to Neuronal Circuits. *Nat. Nanotechnol.* **2012**, *7*, 180−184.
(43) Xie, C.; Hanson, L.; Xie, W.; Lin, Z.; Cui, B.; Cui, Y. Noninvasive Neuron Pinning with Nanopillar Arrays. *Nano Lett.* **2010**, *10*, 4020−4024.
(44) Hanson, L.; Zhao, W.; Lou, H.-Y.; Lin, Z. C.; Lee, S. W.; Chowdary, P.; Cui, Y.; Cui, B. Vertical Nanopillars for in Situ Probing of Nuclear Mechanics in Adherent Cells. *Nat. Nanotechnol.* **2015**, *10*, 554−562.
(45) Berthing, T.; Bonde, S.; Rostgaard, K. R.; Madsen, M. H.; Sørensen, C. B.; Nygård, J.; Martinez, K. L. Cell Membrane Conformation at Vertical Nanowire Array Interface Revealed by Fluorescence Imaging. *Nanotechnology* **2012**, *23*, 415102.
(46) Buch-Månson, N.; Bonde, S.; Bolinsson, J.; Berthing, T.; Nygård, J.; Martinez, K. L. Towards a Better Prediction of Cell Settling

DOI: 10.1021/acsphotonics.6b00126
ACS Photonics 2016, 3, 1208−1216

on Nanostructure Arrays-Simple Means to Complicated Ends. *Adv. Funct. Mater.* **2015**, *25*, 3246−3255.
(47) Krogstrup, P.; Popovitz-Biro, R.; Johnson, E.; Madsen, M. H.; Nygård, J.; Shtrikman, H. Structural Phase Control in Self-Catalyzed Growth of GaAs Nanowires on Silicon (111). *Nano Lett.* **2010**, *10*, 4475−4482.
(48) Mokkapati, S.; Saxena, D.; Tan, H. H.; Jagadish, C. Optical Design of Nanowire Absorbers for Wavelength Selective Photodetectors. *Sci. Rep.* **2015**, *5*, 15339.
(49) Møller, T. C.; Wirth, V. F.; Roberts, N. I.; Bender, J.; Bach, A.; Jacky, B. P. S.; Strømgaard, K.; Deussing, J. M.; Schwartz, T. W.; Martinez, K. L. PDZ Domain-Mediated Interactions of G Protein-Coupled Receptors with Postsynaptic Density Protein 95: Quantitative Characterization of Interactions. *PLoS One* **2013**, *8*, e63352.
(50) Hu, L. A.; Tang, Y.; Miller, W. E.; Cong, M.; Lau, A. G.; Lefkowitz, R. J.; Hall, R. A. Beta 1-Adrenergic Receptor Association with PSD-95. Inhibition of Receptor Internalization and Facilitation of Beta 1-Adrenergic Receptor Interaction with N-Methyl-D-Aspartate Receptors. *J. Biol. Chem.* **2000**, *275*, 38659−38666.
(51) Migaud, M.; Charlesworth, P.; Dempster, M.; Webster, L. C.; Watabe, a M.; Makhinson, M.; He, Y.; Ramsay, M. F.; Morris, R. G.; Morrison, J. H.; O'Dell, T. J.; Grant, S. G. Enhanced Long-Term Potentiation and Impaired Learning in Mice with Mutant Postsynaptic Density-95 Protein. *Nature* **1998**, *396*, 433−439.
(52) Elkobi, A.; Ehrlich, I.; Belelovsky, K.; Barki-Harrington, L.; Rosenblum, K. ERK-Dependent PSD-95 Induction in the Gustatory Cortex Is Necessary for Taste Learning, but Not Retrieval. *Nat. Neurosci.* **2008**, *11*, 1149−1151.
(53) Cahill, L.; Prins, B.; Weber, M.; McGaugh, J. L. Beta-Adrenergic Activation and Memory for Emotional Events. *Nature* **1994**, *371*, 702−704.
(54) Bonde, S.; Berthing, T.; Madsen, M. H.; Andersen, T. K.; Buch-Månson, N.; Guo, L.; Li, X.; Badique, F.; Anselme, K.; Nygård, J.; Martinez, K. L. Tuning InAs Nanowire Density for HEK293 Cell Viability, Adhesion, and Morphology: Perspectives for Nanowire-Based Biosensors. *ACS Appl. Mater. Interfaces* **2013**, *5*, 10510−10519.
(55) Na, Y.-R.; Kim, S. Y.; Gaublomme, J. T.; Shalek, A. K.; Jorgolli, M.; Park, H.; Yang, E. G. Probing Enzymatic Activity inside Living Cells Using a Nanowire-Cell "Sandwich" Assay. *Nano Lett.* **2013**, *13*, 153−158.
(56) Lippincott-Schwartz, J.; Altan-Bonnet, N.; Patterson, G. H. Photobleaching and Photoactivation: Following Protein Dynamics in Living Cells. *Nat. Cell Biol.* **2003**, S7−S14.
(57) Cella Zanacchi, F.; Lavagnino, Z.; Perrone Donnorso, M.; Del Bue, A.; Furia, L.; Faretta, M.; Diaspro, A. Live-Cell 3D Super-Resolution Imaging in Thick Biological Samples. *Nat. Methods* **2011**, *8*, 1047−1049.
(58) KOLASINSKI, K. Catalytic Growth of Nanowires: Vapor−liquid−solid, Vapor−solid−solid, Solution−liquid−solid and Solid−liquid−solid Growth. *Curr. Opin. Solid State Mater. Sci.* **2006**, *10*, 182−191.

DOI: 10.1021/acsphotonics.6b00126
ACS Photonics 2016, 3, 1208−1216